Granular Matter (2025) 27:26
https://doi.org/10.1007/s10035-025-01506-x

RESEARCH

Particulate behaviour of soft granular materials: a case study on lentils

Saurabh Singh[1] · **Beatrice Anne Baudet**[1] · **Matthew Richard Coop**[1]

Received: 24 August 2024 / Accepted: 4 January 2025 / Published online: 17 January 2025

Abstract

In this article, lentils are used as a case study to characterise the particulate behaviour of soft granular materials. Experiments were carried out on a single lentil particle or a pair of lentils. The single particle or a pair of particles in contact were compressed vertically to crushing or to a fixed vertical load. Then, in inter-particle tests, pairs of particles were slid over each other at a constant vertical load, and the tangential stiffness and coefficient of friction were estimated. The pairs of lentil particles in contact were also subjected to repeated normal and tangential loading. The presence or absence of the cover of lentil particles (shell) was found to affect their behaviour significantly under these loading conditions. The lentil particles have a very compliant shell and stiff core in normal loading; the stiffness of the shell is constant, and the core follows Hertz contact law. The lentil particles show less variability in their crushing strength, with high Weibull modulus (~ 10), in comparison to other natural granular materials like sand. With repeated cycles of vertical loading, the contact between a lentil pairs of particles becomes more stiff and less damp. In tangential loading, the coefficient of friction between lentil particles decreases with normal force while the contact stiffness increases. Further, in cyclic tangential loading, the coefficient of friction decreases and the contact stiffness increases with cycles. A simple contact model is also proposed to use in discrete element simulations.

✉ Saurabh Singh
saurabh-singh@ucl.ac.uk

Beatrice Anne Baudet
b.baudet@ucl.ac.uk

Matthew Richard Coop
m.coop@ucl.ac.uk

[1] Department of Civil, Environmental and Geomatic Engineering, University College London, Gower Street, London WC1E 6BT, UK

Graphical abstract

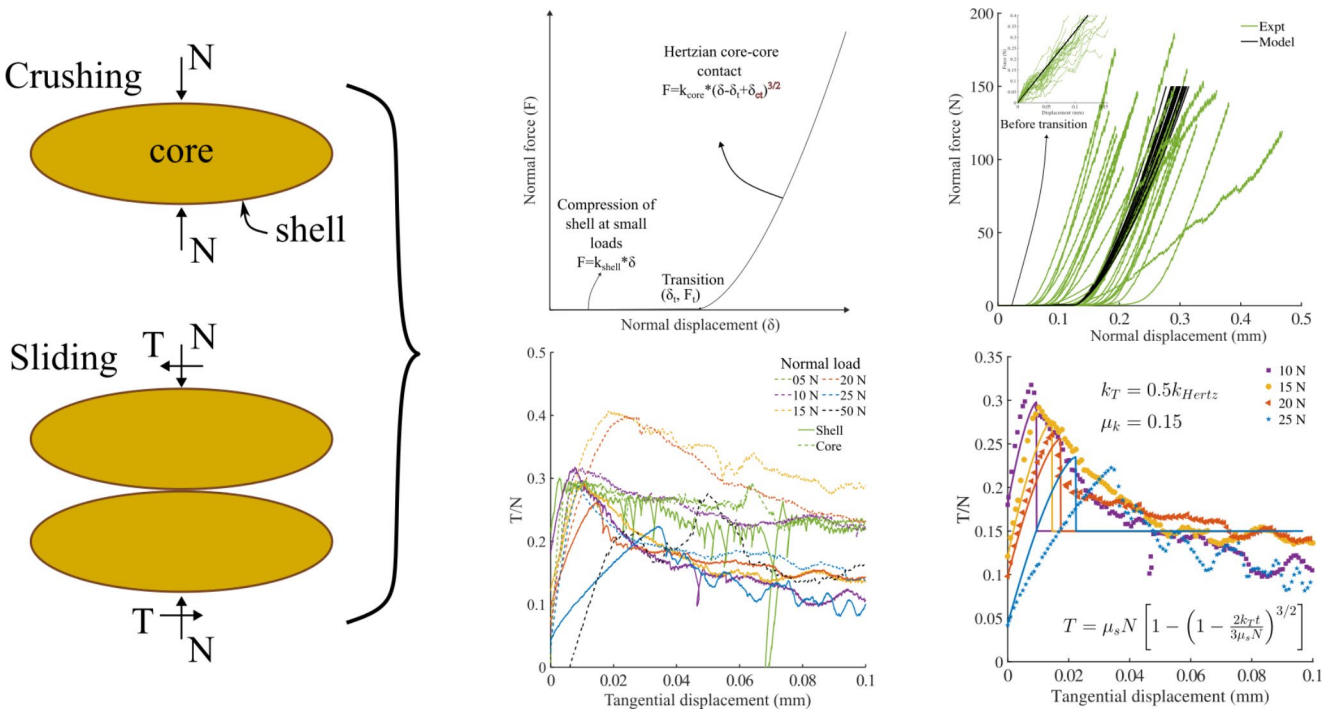

Keywords Particle contact behaviour · Soft granular materials · Coefficient of friction · Normal and tangential stiffness · Crushing strength · Weibull modulus · Layered materials

1 Introduction

A large proportion of food grown worldwide is granular in nature, whether in unprocessed form (e.g. cereals such as wheat, rice, maize, and lentils) or processed (powders) [1]. Managing those at an industrial scale is not without challenges, with problems of flow, segregation or stability [2]. From harvest to storage, via handling and transportation, grains will be subjected to loading events, short- or long-term, monotonic or cyclic, which could cause damage and impact their quality [3, 4]. As for any granular material, the mechanical behaviour of those foods will be governed by the properties at the grain scale [5, 6]. Their two- to three-phase nature adds to their complex behaviour, whether they contain solids and gas when dry or solids and water when fully saturated, or solids, gas and water when partially saturated. To be able to develop competent predictive tools for granular foods would help create a more sustainable food industry with less waste, as well as being economically beneficial.

In areas of engineering such as chemical engineering or geotechnical engineering, the discrete element method (DEM) has been used and developed since the seminal paper of Cundall and Strack [7] to simulate granular materials as a system of discrete particles. DEM has evolved from using spheres with simple contact laws to more sophisticated grains of realistic shapes with elasto-plastic contact behaviour, e.g. [8]. A review of the use of DEM for agricultural granular materials was published in 2016 by Horabik and Molenda [9]. It is now well accepted that in order to develop better models, the database for experimental data at the particle scale needs extending. To this aim, this paper presents results from a series of single particle and inter-particle tests performed on lentil seeds, bringing insight into their internal strength, and normal and tangential contact behaviour. With the reasonable repeatability of their shape, lentils have the double advantage of being a simple material to simulate the shape of in DEM as well as to implement improvements to contact models traditionally developed for spheres [10]. A recent set of studies [11, 12] used lentils as a model material for calibration of DEM algorithms, wherein they performed in-situ triaxial compression tests with x-ray computed tomography (XCT) to capture the kinematics and deformation of lentils at various stages of triaxial compression stress path. The contact model used in DEM simulation in this study [12] was very simplistic and not appropriate for lentils, as will be shown in this paper.

Research on cereals and pulses predates this later research, of course, being a substantial part of food production and market. The time-dependent behaviour of grains, in particular stress relaxation, has been pointed out as an important factor in grain damage. For example, Bargale et al. [13] conducted experiments in which lentils were compressed between two platens at a controlled deformation rate to determine their compressive strength, elastic parameters and relaxation modulus, with a main focus on the effect of moisture content. These parameters, however, were derived from equations adapted from contact models rather than directly from the test data. A similar approach was undertaken by Shelef and Mohsenin [14] for determining the modulus of elasticity of wheat grains. Although providing a useful set of values for further analyses, the reliance on models that were developed for other types of materials presents severe limitations. Many of the advances in granular material testing and modelling have been achieved in the area of soil mechanics, with unique particle-to-particle experiments [15–19], or more realistic model grains and contact laws [8]. The approach followed by Antonyuk et al. [20] on grain breakage presented analogies to research carried out on sands, see [21], but this presents an extreme form of deformation while the pre-failure deformation, presented here, is neglected.

This article presents a detailed quantification of mechanical behaviour of single lentils under monotonic and cyclic normal loading, and contact between pairs of lentils under monotonic and cyclic loading along normal and tangential directions. The shell-core structure of lentils is systematically studied, and its effect on their mechanical behaviour is clearly demonstrated. Under compression, the variability of crushing strength of lentils is investigated using Weibull statistics. To aid the DEM simulations of lentils, a simple, yet comprehensive, model for their normal and tangential contact behaviour is presented. Further, this study also extends the dataset available for contact mechanics of layered materials such as layered composites and contacts in presence of protective coating [22, 23].

2 Materials and methods

A set of ellipsoidal lentil particles, with major and intermediate diameters that were similar at (6.26 ± 0.34) mm and minor diameters/thicknesses of (2.37 ± 0.14) mm, were tested for single particle crushing strength and the inter-particle contact behaviour of two particles. The red lentil particles used in this study were of the same type and from same source as those used in the in-situ XCT triaxial compression study performed by Pinzon et al. [11].

Lentil particles are composed of a skin (referred here as the shell of the lentil) of thickness 50 µm to 150 µm and a core with two halves of the lentil in contact with each other. The lentil shell keeps the core intact and is in non-adhesive contact with the core. The modulus of elasticity of lentils varies significantly in the literature (200 MPa—[13]; 1200 MPa—[24]) and the Poisson's ratio of lentil is suggested to be 0.30 [24]. The lentils, tested in this study, had a moisture content of 2.5%.

An apparatus, designed for inter-particle contact behaviour testing, was used for crushing and sliding experiments [25, 26]. Figure 1a and b show schematic drawings and a photograph of this apparatus. The apparatus has two horizontal arms and a vertical arm to apply horizontal loads and a vertical load. Each arm has a linear actuator with a 60 mm travel distance and step size of 0.198 µm, a load cell with capacities of 1 kN and 0.5 kN in vertical and horizontal directions respectively and with resolutions of 0.02 N and 0.01 N, and a proximity type displacement transducer with a resolution of 10 nm and a working range of 4 mm. The horizontal arms are connected to a sled which moves freely on six hardened steel ball bearings. The base platen is mounted on the sled and the top platen is mounted on the vertical load cell. The horizontal arms are designed to move independently of each other, with linear bearings connecting them to the sled. Two microscope cameras are used to capture pictures from two horizontal directions.

Before the start of each test, the lentil dimensions were either measured with a Vernier caliper for the crushing tests, or for the inter-particle contact tests a three-dimensional surface profile of the particle was mapped using a Zeiss optical stereoscope. For single particle crushing, the lentil was placed on the base platen and the top platen was brought in contact with the particle and compressed further under displacement control at a rate of 1.2 mm/h (Fig. 1c). The test was stopped when the strength dropped significantly, i.e. by around 10% of the previous load, which was defined as the point of crushing. A total of 30 experiments were performed for single particle crushing.

While for the single particle crushing tests the particle was unrestrained at the platen contacts, for the inter-particle contact behaviour tests, two particles were glued with Araldite standard resin and hardener (mixed at 1:1 proportion) on the top and base platens and cured overnight in air. The platen with the base particle was mounted on the sled, and the platen with the top particle was mounted on the vertical load cell (Fig. 1d). The vertical arm was then brought down slowly in a manual control mode at a rate of 0.01 mm/s, to bring the two particles into proximity. The top particle was then moved at a speed of 0.1 mm/h under displacement control mode to establish contact, after which it was compressed further to the desired vertical load. The

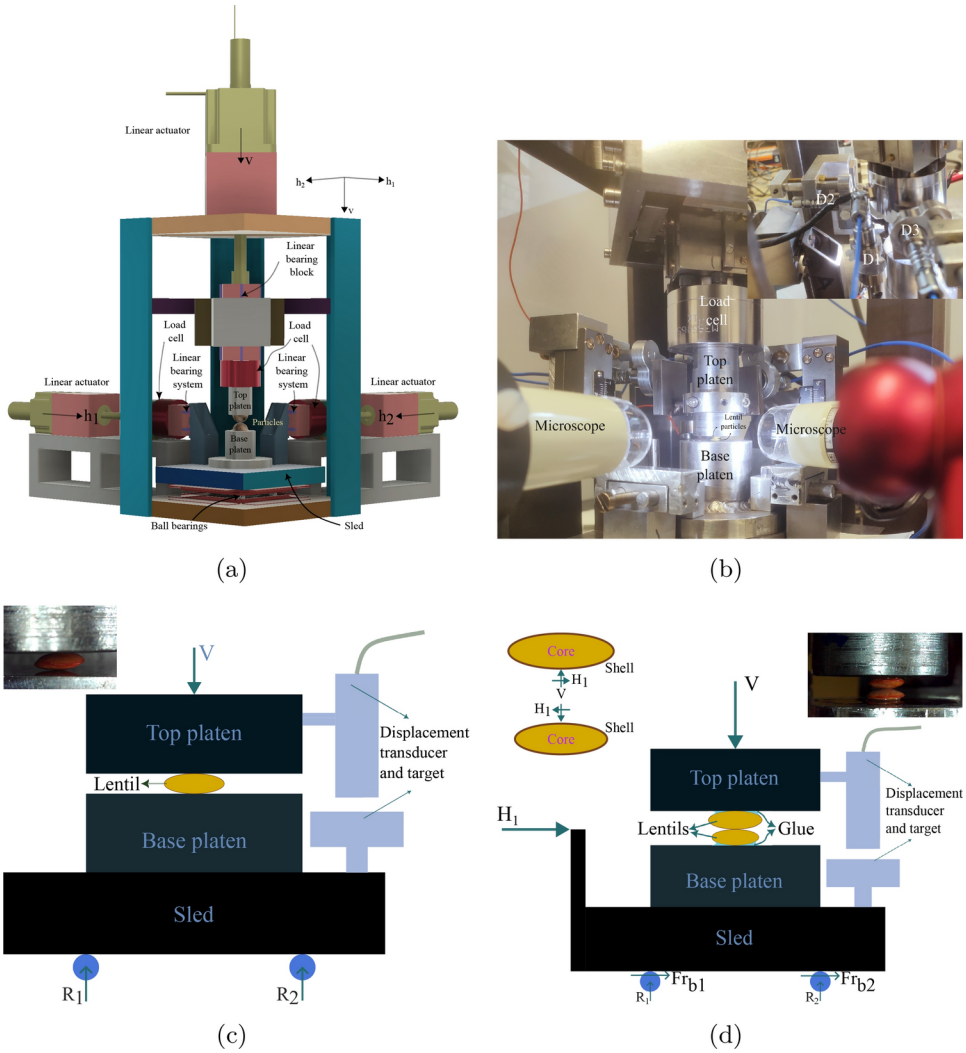

Fig. 1 Description of inter-particle apparatus, crushing of single particle and sliding test. **a** Schematic of inter-particle apparatus (h_1—horizontal direction 1, h_2 - horizontal direction 2, v—vertical direction). **b** Experiment on lentil (D1: vertical displacement transducer, D2: horizontal displacement (h_1) transducer, D3: horizontal displacement (h_2) transducer). **c** Schematic of single particle crushing (V: vertical load, R_i - reaction on the ball bearing from the base). **d** Schematic of inter-particle test (V: vertical load, H_1: horizontal load along h_1, Fr_{b1} and Fr_{b2}: frictional forces ($\ll H_1$) on the ball bearings)

speed was chosen so that the initial force at first contact was less than 0.05 N. After the desired vertical load was achieved, the base particle was moved horizontally at a speed of 0.1 mm/h to a maximum displacement of 0.1 mm for tangential shearing at a constant vertical load. After monotonic tangential shearing, cyclic tangential loading (forward and backward motion of the horizontal arm) was performed with ± 0.1 mm amplitude from the initial contact point, at a speed of 0.2 mm/h (i.e. 2 h/cycle) to assess the change in stiffness and coefficient of friction between the lentil particles during repeated loading. A total of 11 inter-particle contact behaviour tests were conducted, out of which five were performed on the lentils with shell, and the remaining six tests were conducted on the lentils with only core by removing the shell.

Further, a few tests (other than described above) were performed to assess the cyclic normal loading response of a single and a pair of lentils with the shell.

3 Data collection and analysis of data

The inter-particle apparatus records vertical displacements v (mm), horizontal displacements h_1 (mm) and h_2 (mm), along with vertical load V (N), and horizontal loads H_1 (N) and H_2 (N). In single particle crushing experiments, the horizontal displacements are kept at zero and any horizontal loads arising from the topography of the lentils contact is measured, in addition to the vertical displacement and vertical load. The resultant of H_1, H_2 and V is calculated as the resultant normal force N (which was approximately equal to V); similarly, the resultant of h_1, h_2 and v are calculated as the resultant normal displacement n (as h_1 and h_2 were zero, n was equal to v). The tensile stress σ on a vertical plane with its normal perpendicular to the direction of loading is calculated from the resultant normal force as [15, 27]:

$$\sigma = \frac{0.9\,N}{d_I\,d_m} \tag{1}$$

where d_I and d_m are the intermediate and minor diameters of the particle, respectively. For lentils with an approximate ellipsoidal shape, the major and intermediate diameters are approximately equal. The tensile strength of thirty lentil particles (i.e. the peak tensile stress at failure) was used to calculate the probability of survival (P_s):

$$P_s(\sigma) = \frac{\text{Number of particles with strength greater than } \sigma}{\text{Total number of particles}} \tag{2}$$

and the Weibull modulus (m), by fitting the Weibull distribution for survival statistics:

$$P_s(\sigma) = \exp\left[-\left(\frac{\sigma}{\sigma_0}\right)^m\right] \tag{3}$$

where σ_0 is the characteristic strength at which $\ln(\ln(1/P_s))$ is zero (corresponding to P_s of $\exp(-1)$).

For both inter-particle contacts and single particle crushing tests, the normal loading behaviour is compared with the Hertz prediction which requires the modulus of elasticity (E), Poisson's ratio (ν), and radius of curvature (R) at the contact of bodies. For the single particle crushing tests, there are two contacts of the lentil particle with the flat top and base platens. These are made of mild steel, for which the modulus of elasticity and Poisson's ratio were taken as 220 GPa and 0.30, respectively. In the inter-particle tests, there is only one non-adhesive contact between the two lentil particles. The displacement/deformation at the lentil to platen bond interfaces, in inter-particle tests, may be assumed to be zero because of the wide expanse and small thickness of the glued surface (compliance of the vertical and horizontal arms between the points of displacement measurements for a glued metal block between top and base platen was 1 nm/N and 48 nm/N which was accounted for before analysing the data). However, for inter-particle tests on lentils with shell, an extra source of compliance is encountered due to presence of shell between core and glue/platen for both top and base particle. For these six inter-particle tests on lentils with shell, an additional compliance correction was performed for normal loading response. The radius of curvature of the platens is infinite, and the radius of curvature of the lentil particles was calculated by fitting a circle on the image of the particle in the area within 1 mm of the contact. For each lentil particle, two radii of curvatures are calculated using images from h_1 and h_2 microscopes and the radius used in the calculations was taken as the harmonic mean (inverse of arithmetic mean of curvatures).

In the monotonic vertical loading stage of the inter-particle contact behaviour test, the resultant normal force and normal displacement are calculated as described for the crushing test, but the contact between the two lentils often being not quite horizontal gave rise to greater horizontal loads which were negligible for crushing tests. In the tangential loading tests (both monotonic and cyclic), the tangential loading is done only along the h_1 direction while keeping the h_2 displacement at zero and the vertical load constant. For tangential loading, it is important to calculate the direction of tangents at the contact point along both h_1 and h_2 directions so that normal and tangential forces (N and T_1) can be obtained at the contact (instead of the vertical and horizontal forces). The tangents at the contact point are obtained using the measured $h_1 - v$ profile $\left(\frac{dh_1}{dv}\right)$ determined later during the test when sliding failure occurs with equilibrium along the h_2 direction ($T_2 = 0$). Using these tangents, the contact normal force (N) and tangential force (T_1) along with normal (n) and tangential displacements (t_1) are obtained in the direction of sliding. From these forces and displacements, the normal stiffness $\left(\frac{\partial N}{\partial n}\right)$ and tangential stiffness $\left(\frac{\partial T_1}{\partial t_1}\right)$ are calculated. In the tangential shearing, prior to sliding failure, the vertical displacement measurements are affected by a compliance of vertical arm along the lateral direction. This introduces an error in the slope of $h_1 - v$ profile before sliding, so the slope before sliding is assumed to be equal to the slope at onset of sliding.

4 Lentil behaviour under normal loading

The force-displacement behaviour of lentils is presented in Fig. 2. It consists of the initial response due to compression of the shell followed by deformation of the core as shown in Fig. 2a. The transition of shell to core response is clearly visible, in the form of a knee in the force-displacement plot, due to significant difference in the stiffness of the shell and the core. This transition happens at different force levels, (0.44± 0.27) N with a linear relation ($F_t = 3.43\delta_t$) between the transition force and transition displacement (Fig. 2b). The lentil behaviour prior to the transition (response of shell) is plotted in Fig. 2c. The response of the shell is quite linear with average slope of (3.26± 1.56) N/mm. Following the compression of the shell, the force required to compress the core grows with approximately 1.5$^{\text{th}}$ the power (as in Hertz contact theory) of the deformation $\left(F \propto \delta^{1.65\pm0.19}\right)$ as shown in Fig. 2d, until the failure of the lentil particle (defined as a rapid drop of more than 10% in the force, refer to inset of Fig. 2a). In Fig. 2d the displacement up to transition, which are dominated by the shell, have been deducted, so the core response for different tests can be better compared. Several small drops in the normal force are observed in a few tests prior to the initial major failure; and after the failure, the apparent strength again increases till complete damage to the lentil particles, as shown in the inset of

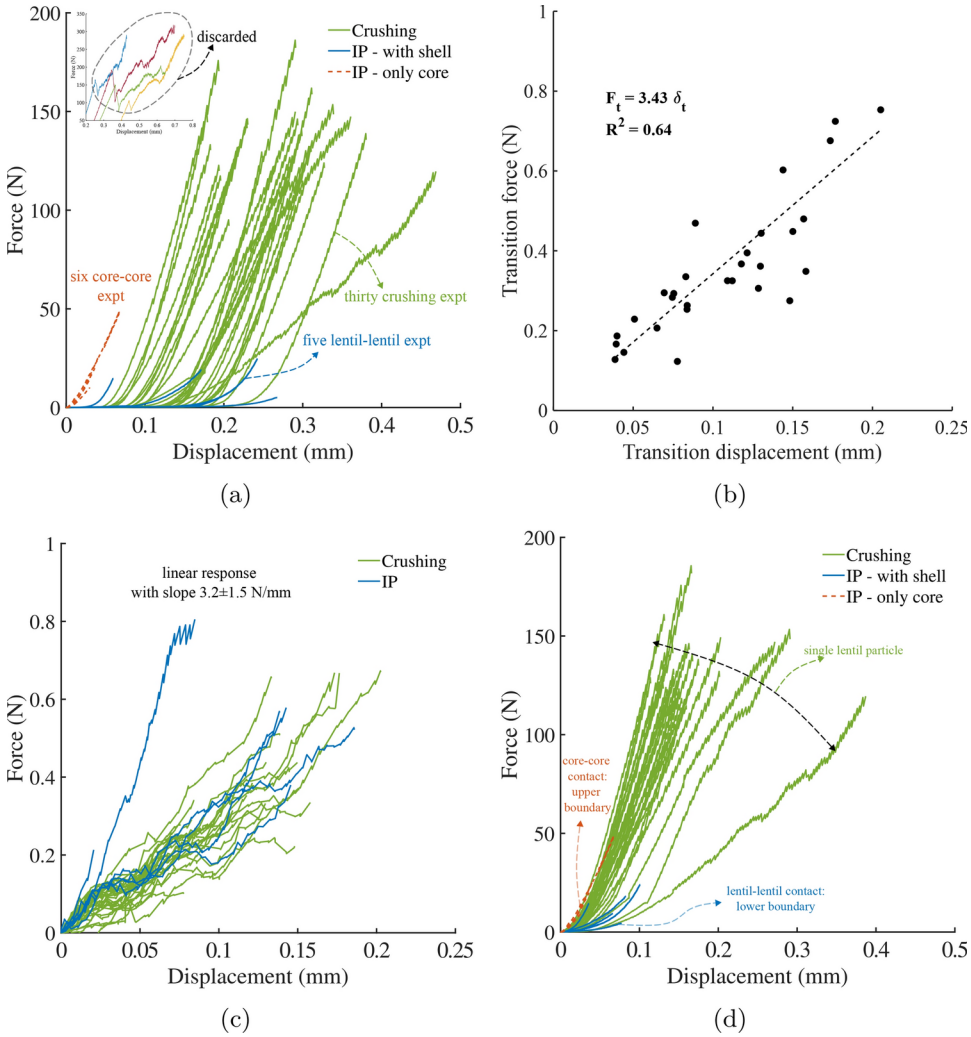

Fig. 2 Force–displacement behaviour of lentils in single particle normal loading tests to crushing failure and inter-particle tests (IP). **a** Complete response (only core-core experiments were without shell). **b** Identification of transition from shell to core. **c** Response of the shell. **d** Response of the core

Fig. 2a. Only a few tests were carried out to complete damage, the rest were stopped just after the initial major failure. Images of typical lentil particles are shown in Fig. 3, before test (Fig. 3a) and after test (Fig. 3b–f). In a test where lentils were tested till complete damage, the lentil particle broke into several pieces, as shown in Fig. 3e and f. The tests carried out only till initial major failure did not show damage on the surface of lentil (Fig. 3b and d) except a few in which cracks are seen on the surface (Fig. 3c).

Figure 4 presents the stiffness-force behaviour in log–log plots of lentils under normal loading in single particle crushing and the inter-particle tests between two particles. The two tests are equivalent in normal loading because in the single particle crushing test the particle is in contact with two rigid platens while in the two particles contact test the displacement at the particle-particle contact will be approximately double that on the particle-platen contact of the crushing tests. The stiffness is almost constant at low loads for the majority of the tests that had the shells in place and then increases quite rapidly to become linear in the $\log - \log$ plot $\left(\text{stiffness} \propto F^{0.39\pm0.06}\right)$. Figure 4a also shows that the lentils shell and core behave quite uniformly. The stiffness of the lentil before transition, i.e. the shell, lies between 1 N/mm to 5 N/mm (Fig. 4b). Figure 4c shows only the post-transition behaviour of the core, which is linear in the log–log plot. The data points with unfilled markers are for the tests on particles with the shells removed, and the stiffness starts at quite a high value and follows the post-transition behaviour of lentils. For all the tests, radii of curvatures were measured using the microscope images and the Hertz model was used to obtain predictions. Figure 4d shows the normalised stiffness (the ratio of the stiffness from the experiment and that predicted by Hertz) after transition. At low loads, the response deviates from Hertz due to the influence of the shell and asperities of the core; however, at higher loads, the normalised stiffness is close to 1 (on average 1.5). For inter-particle experiments with only core, the normalised stiffness remains close to 1 (on average 1.5) from the start of the test.

The tensile strength of the lentils (using the normal force at failure) was calculated using Eq. 1, and with these strengths, the probability of survival (using Eq. 2) is estimated.

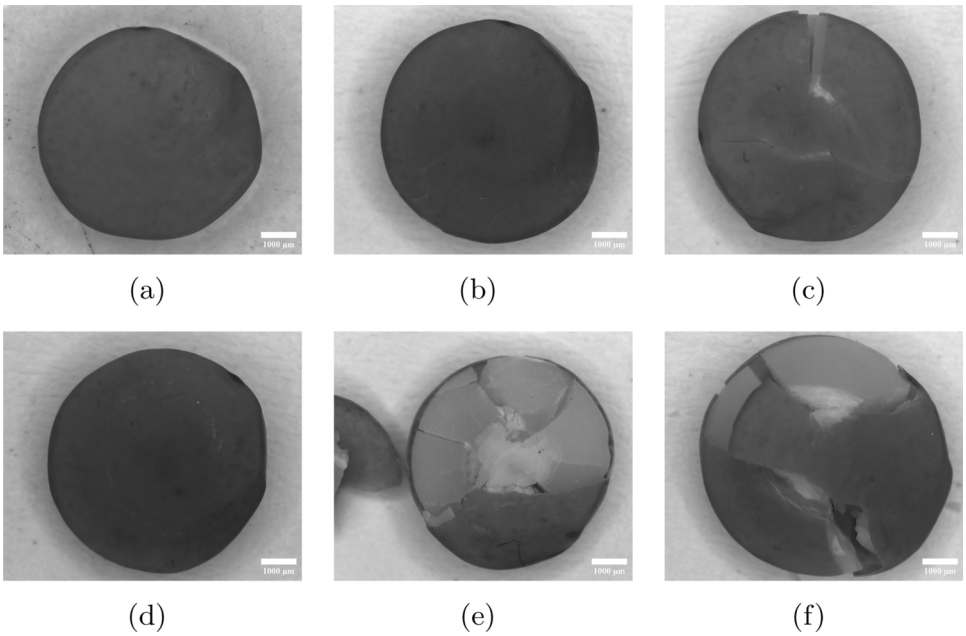

Fig. 3 Lentil particles before and after testing. **a** Before testing; **b**, **c** and **d** loaded to first major failure; **e** and **f** loaded to complete damage

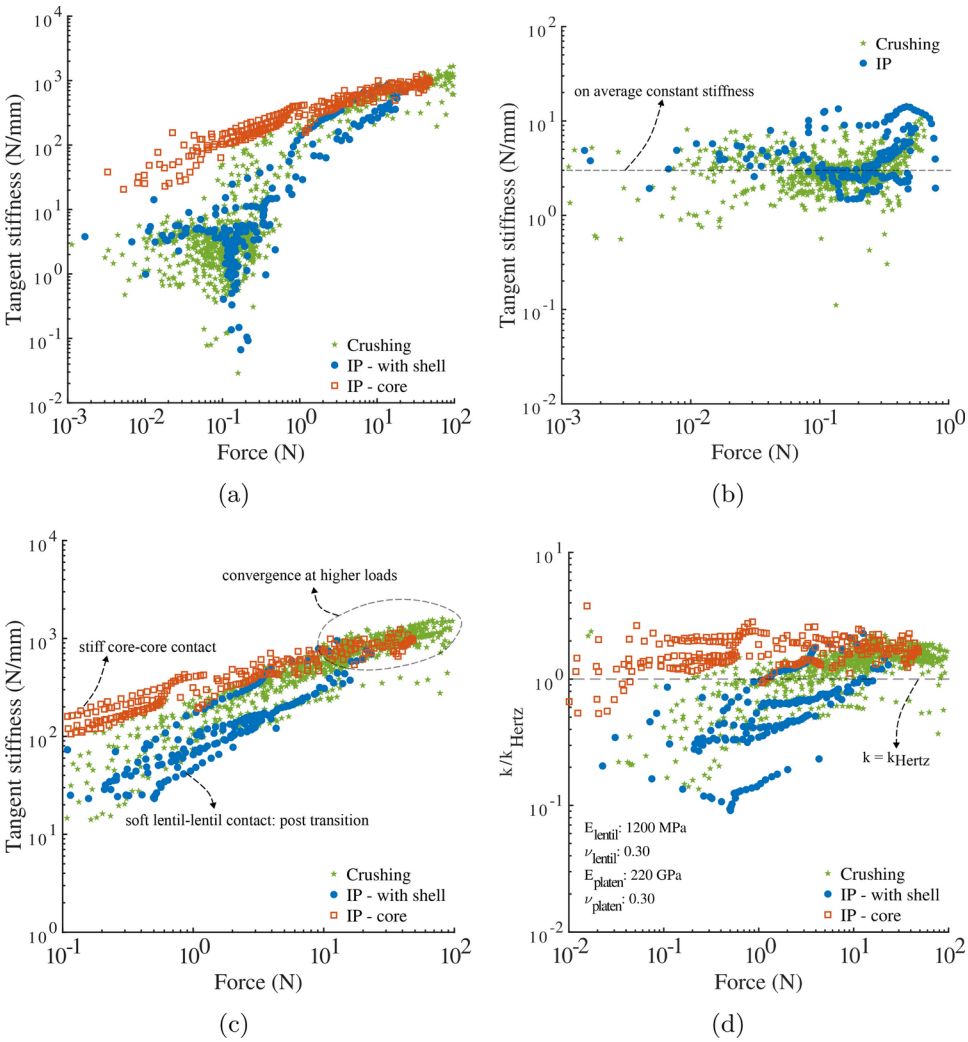

Fig. 4 Stiffness-force behaviour of lentils in single particle crushing tests and inter-particle normal loading tests (IP). **a** Complete test. **b** Stiffness of the shell. **c** Stiffness of the core. **d** Comparison with Hertz prediction of the stiffness

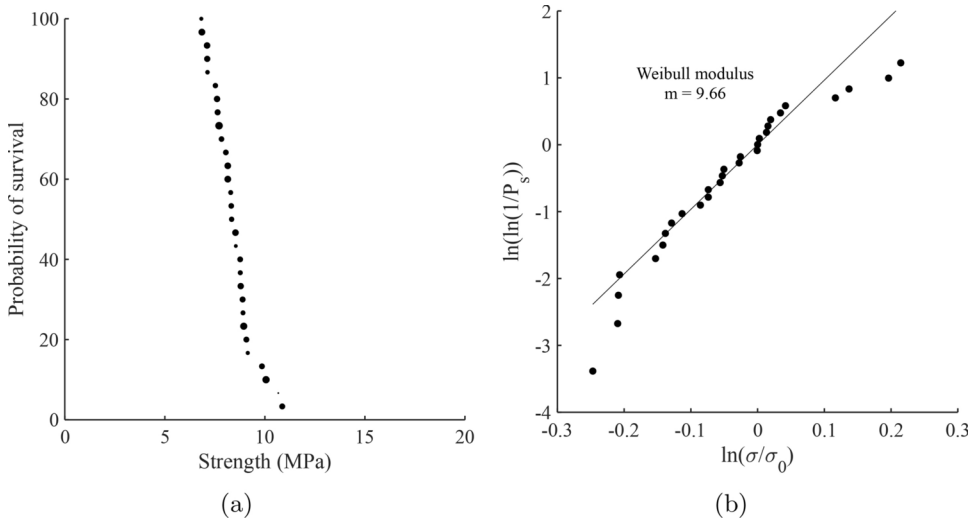

Fig. 5 Probability distribution in single particle crushing tests. **a** Probability of survival of a lentil in compression (the size of markers is proportional to minimum cross section area of the lentil). **b** Weibull modulus

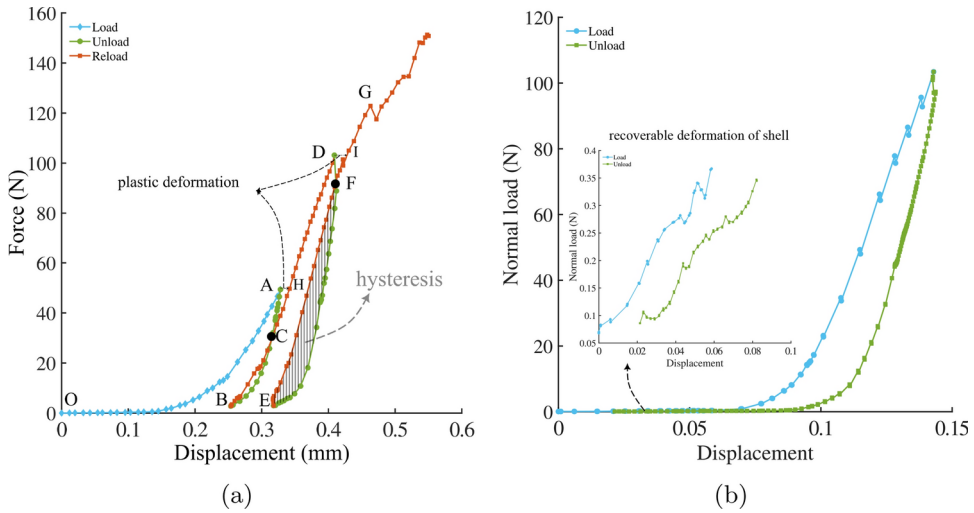

Fig. 6 Unload-reload behaviour of lentil with shell under normal loading. **a** Lentil pair with shell. **b** Single lentil with shell

Figure 5a shows the probability of survival against tensile strength. All the lentil particles survived a tensile stress of about 6 MPa and failed at less than 13 MPa, half of the lentil particles survived a tensile stress of 8.3 MPa. The characteristic strength (σ_0) of the lentil particles (at $P_s = \exp(-1)$) was 8.8 MPa. The size of markers in Fig. 5a is proportional to the minimum vertical cross-section area of the lentil. Nakata et al. [28] have shown that the probability of survival curve shifts towards the left with increase in particle size for a typical sand (Aio sand); in our research, the sizes of lentils were not so distinct to see a clear segregation of larger particles and smaller particles. The Weibull's modulus, refer to Eq. 3, was obtained by fitting a straight line on the $\ln\left(\ln\left(\frac{1}{P_s}\right)\right)$ vs $\ln(\sigma_0)$ plot as shown in Fig. 5b, from which the Weibull modulus m was found to be 9.66 for lentils which is much higher in comparison, for example, to typical coarse grained soils (1.5 to 3.0 for Leighton Buzzard quartz sand and 1.0 to 1.5 for a decomposed granite sand [27], 4.2 for a quartz sand, 1.8 for a feldspar sand [29]. This suggests that the tensile strength of lentils is much more uniform than for sands, which can be attributed to the more uniform shapes of lentils, while in sands, the particle geometry along with internal defects (mineral boundaries and micro-fissures) can contribute to non-uniform crushing strengths. The irregular geometry of sands can give rise to stress concentrations at the platens and also rotation and sliding at the contact points which cause unknown frictional forces on the platen in a traditional apparatus [15]. In addition, internal defects in some sand grains can cause random planes of weakness in the particle [27].

5 Lentil behaviour under cyclic normal loading

Figure 6a and b shows a typical unload-reload plot of lentil with shell under normal loading in inter-particle and single particle tests, respectively. On the first loading, the shell deforms to 0.08 mm to 0.12 mm followed by power law increase in the strength of lentil. In the inter-particle test, the

lentil pair was unloaded at 50 N, reloaded to 100 N, unload and reloaded to 150 N at which failure was observed. For each unload-reload response, a small plastic deformation is observed (associated to creep) as shown by arrow AH and arrow DI in Fig. 6a. From the unload response in Fig. 6a, it is not clear if the response of the shell is elastic or plastic as unloading is done till 2 N. In the single particle test, as shown in Fig. 6b, the lentil particle was unloaded to 0.05 N which is below the point of transition. The response of lentil is found to be elastic as shown in the inset of Fig. 6b, although, the core response shows plastic deformation.

A cyclic normal loading test was performed on a pair of lentil particles with shell to assess the effect of repeated normal loading on the behaviour of lentils. Lentil particles were loaded to different mean normal loads and subjected to an amplitude of 5 N cycle with 0.25 h of cycle period. Figure 7 presents the results of typical cycles (Fig. 7a), secant stiffness with cycle number for each mean normal load (Fig. 7b), damping with cycle number for each mean normal load (Fig. 7c), and damping and stiffness of fifth cycle with mean normal load (Fig. 7d). Figure 7a shows the force displacement response from all the cycles at different normal loads. The inset in Fig. 7a highlights the cycles corresponding to normal load of 10 N. Two set of plastic deformation were observed, plastic yielding in monotonic loading and fatigue during cyclic loading. The rate of monotonic yielding with unit increment in force decreases with increase in normal force as shown by solid arrows (a, b, c, d, e, f) in Fig. 7a. Also, fatigue decreases with increase in cycles as shown by the gaps of consecutive cycle in the inset of Fig. 7a which hints towards cycles reaching a plastic shakedown. For each cycle, the secant stiffness was calculated using the slope of a line fitting the points of the hysteresis and damping was calculated by the ratio of area of hysteresis (energy loss) to the area of the triangle formed with x-axis and hysteresis diagonal (stored elastic energy). The stiffness of lentil contact in normal loading increases with cycle number for all mean normal loads (Fig. 7b) and similar response was observed for damping except for mean normal load of 10 N where damping first increases and decreases after reaching a peak (Fig. 7c). The secant stiffness increases with mean normal load (Fig. 7b), however, damping decreases with mean normal load (Fig. 7c). The trend of this change in stiffness

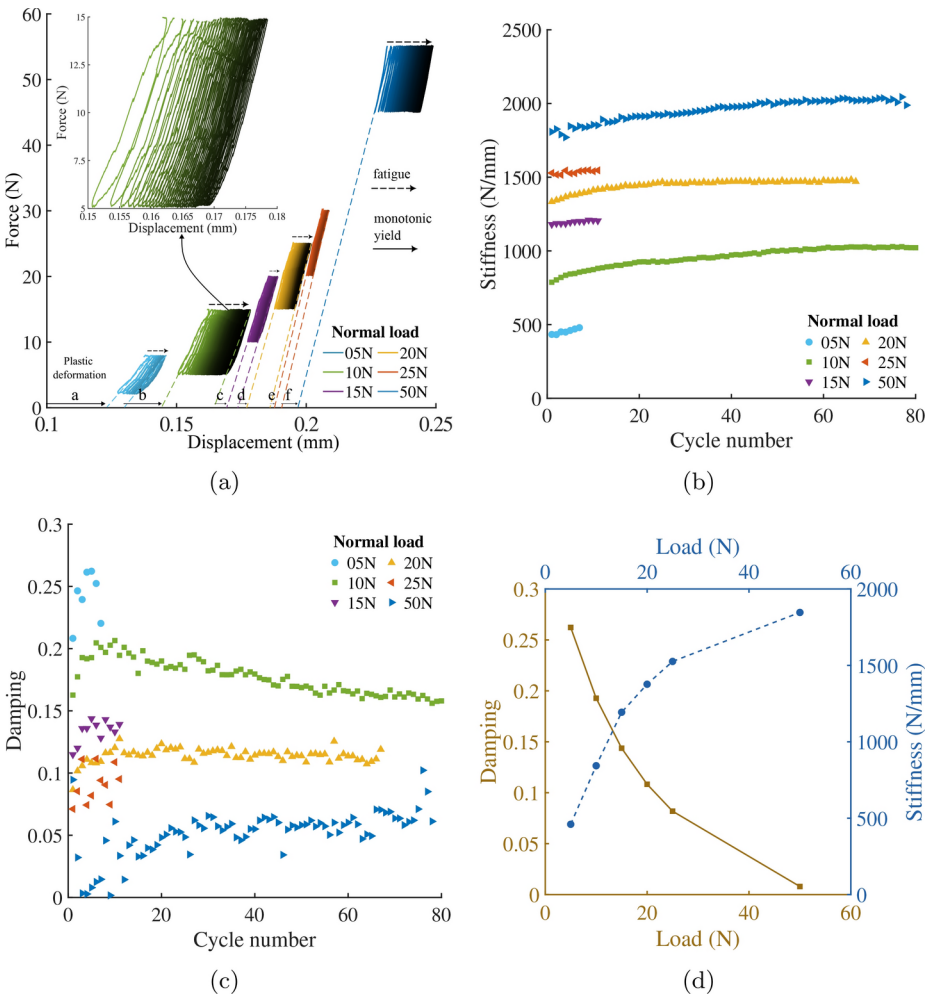

Fig. 7 Cyclic normal loading on a pair of lentil particles with shell at different mean normal loads and amplitude of 5 N. **a** Normal load with displacement (cycle number increases from light to dark colour for each mean normal load). **b** Secant stiffness with cycle number. **c** Damping with cycle number. **d** Damping and secant stiffness of 5th cycle with mean normal load

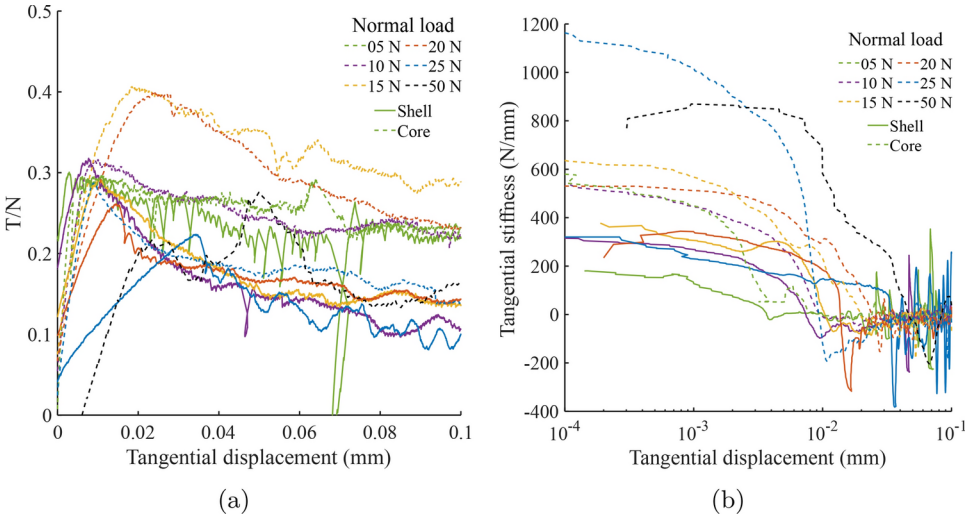

Fig. 8 Tangential contact behaviour of lentil particles. **a** $\frac{T}{N}$ with tangential displacement. **b** tangential stiffness with tangential displacement

Table 1 Coefficients of friction and stiffness of lentils in monotonic tangential loading (normal load: N, static friction: μ_s, displacement at static friction: d_p, kinetic friction: μ_k, sliding displacement: d_s, k_T : tangential stiffness)

Description	N (N)	μ_s (d_p μm)	μ_k (d_s in μm)	k_T at 1 μm
With shell	5	0.30 (03)	0.23 (15)	128
With shell	10	0.32 (08)	0.13 (40)	268
With shell	15	0.29 (10)	0.14 (52)	307
With shell	20	0.26 (15)	0.16 (26)	342
With shell	25	0.22 (34)	0.12 (42)	230
Core	5	0.30 (11)	0.25 (14)	449
Core	10	0.32 (10)	0.24 (30)	444
Core	15	0.41 (18)	0.34 (32)	567
Core	20	0.40 (24)	0.26 (58)	512
Core	25	0.29 (09)	0.14 (25)	1018
Core	50	0.28 (50)	0.15 (84)	869

and damping with mean normal load is shown in Fig. 7d for the fifth cycle of each test.

6 Lentil behaviour under monotonic tangential loading

After normal loading, in the inter-particle tests, the lentil particles were sheared along the tangential direction at a constant vertical load. Figure 8a and b present the ratio of tangential load to normal load $\left(\frac{T}{N}\right)$ with tangential displacement and tangential stiffness with tangential displacement. The non-zero tangential force at the start of tangential loading is the result of the slope of contact in the h1-v plane, which is assumed to be constant prior to sliding. The tangential load increases with displacement to a peak and then drops to a constant value (steady state).

Table 1 presents the summary of results of all monotonic tangential tests. The coefficient of static friction, μ_s, is the peak of T/N and coefficient of kinetic friction, μ_k, is the average of T/N over the range of tangential displacements from the onset of sliding (d_s in Table 1) to 100 μm. The displacement at the peak T/N (d_p) increases with the increase in normal load. For lentils with shell, μ_s reduces with increase in normal load (Fig. 9a); however, μ_k appears to be constant at 0.15(±0.04). For the lentils without shell, there is no correlation between coefficient of friction and normal load; μ_s is 0.33(±0.06) and μ_k is 0.23(±0.07).

Figure 8b shows the reduction of tangential stiffness with tangential displacement in a semi-log plot. Initial tangential stiffness increases with increase in normal load for particles with and without shells, as can be seen in Figs. 8b and 9b. Table 1 also gives a list of tangential stiffness at 1 μm displacement for different normal loads. The tangential stiffness for lentils with shell is significantly less than that of the sands which is typically around 500 N/m to 1000 N/m at 1 μm displacement for normal loads 5 N to 25 N; and the coefficient of friction of lentils with shell is similar to smooth Leighton Buzzard sand which is around 0.2 [19].

7 Lentil behaviour under cyclic tangential loading

After monotonic shear, the lentil particles were subjected to cyclic tangential loading. Figure 10 shows the response of a lentil particle core pair in a typical cyclic tangential loading test performed at a normal load of 50 N and with an amplitude of 100 μm tangential displacement from the mean position. The top particle was kept fixed laterally, and only vertical movement was allowed, whereas the base particle was displaced 100 μm backward and forward from the mean position. During the test, the vertical load was kept at 50 N; after resolution of the forces, the normal load was also approximately 50 N (Fig. 10a). At the start of

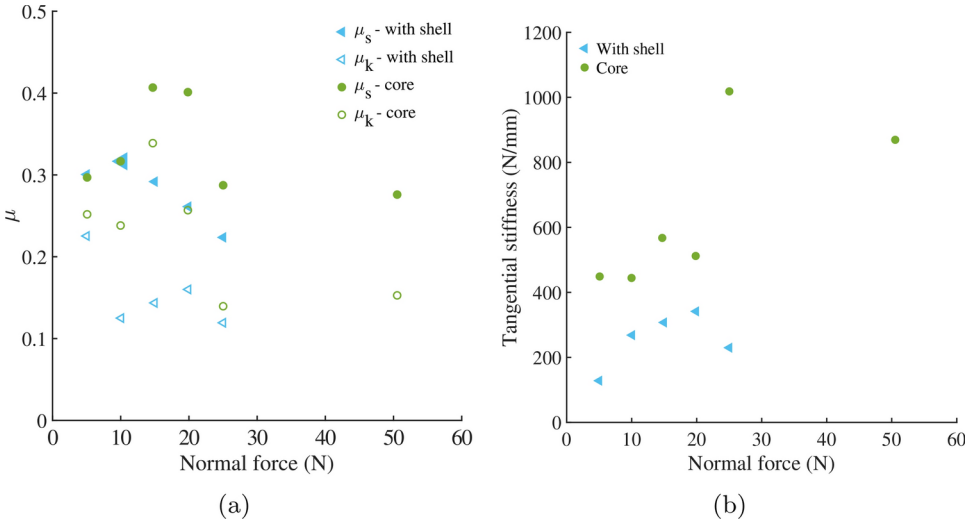

Fig. 9 Influence of load level on **a** coefficients of friction, and **b** tangential stiffness at 1 μm

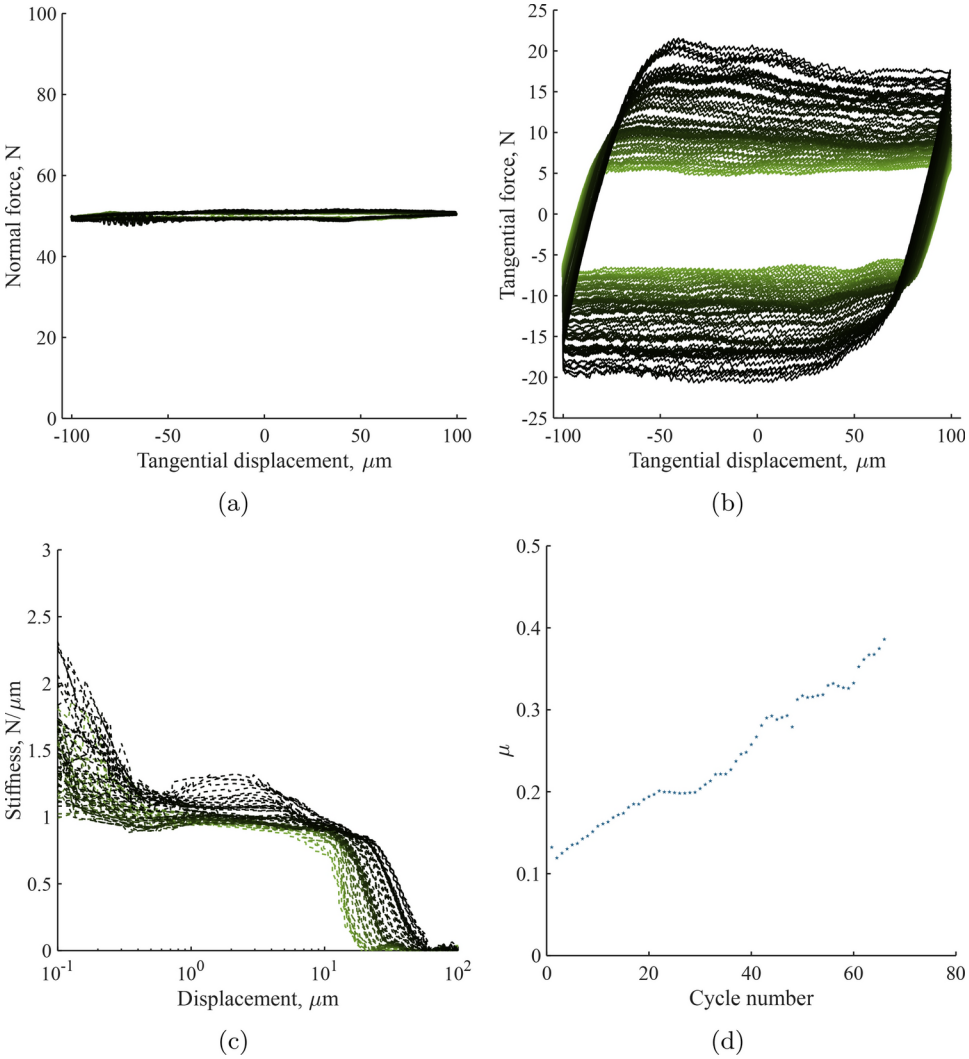

Fig. 10 A typical cyclic tangential loading test on lentil cores under 50N normal load. **a** Normal load during cyclic loading. **b** Evolution of tangential force with tangential displacement (cycle number increases from light to dark colour). **c** Tangential stiffness degradation in forward displacement of base particle. **d** Coefficient of friction

cyclic tangential shearing, the base particle was displaced backward, and the tangential force drops from positive to zero to negative prior to sliding in the backward direction (Fig. 10b). At the onset of sliding, the tangential force tends towards a constant value, which changes with the cycles. On the reversal of the movement, the tangential force increases from negative to zero to a positive value and sliding again occurs at constant tangential load. In Fig. 10b the data are coloured from light to dark green as the number of cycles increases.

Figure 10c shows the degradation of tangential stiffness during the reversals of loading. With the increase in cycle number, the stiffness increases and the displacement at the onset of sliding (where stiffness goes to zero) also increases. Figure 10d shows the increase in the coefficient of friction with cycle number. This is averaged over 150 µm of sliding displacement for the central part of each cycle in the forward and backward direction (an average between forward and backward also being taken).

Figure 11 shows the degradation of cyclic stiffness in all the tests. Figure 11a and b are the responses for tests done with shells, and Fig. 11c and d are for core only tests. For all the tests, tangential stiffness increases with cycles and with normal load. However, for several tests on lentil cores the tangential stiffness at the start of loading has quite a low value, which increases initially before decaying. The stiffness of the lentil cores is much higher in comparison to the lentil shells (compare Fig. 11a with c and Fig. 11b with d). Also, with the increase in normal load, the onset of sliding happens at larger displacements, i.e. where tangential stiffness goes to zero. This increase is more apparent for core only tests than tests done with shells. Figure 12 presents the cyclic stiffness (at 1 µm) and the cyclic coefficients of friction (μ) with the cycle number for different normal loads. The filled markers represent tests done with shells, and empty markers represent tests done on lentil cores. From Fig. 12a, the stiffness at the reversal of each cycle generally tends to increase with cycle number and with the increase in normal load. However, in both cases, there are a few exceptions. The coefficient of friction generally drops with cycle number and with increase in normal load, again with a few exceptions (Fig. 12b) and is much higher for the core only

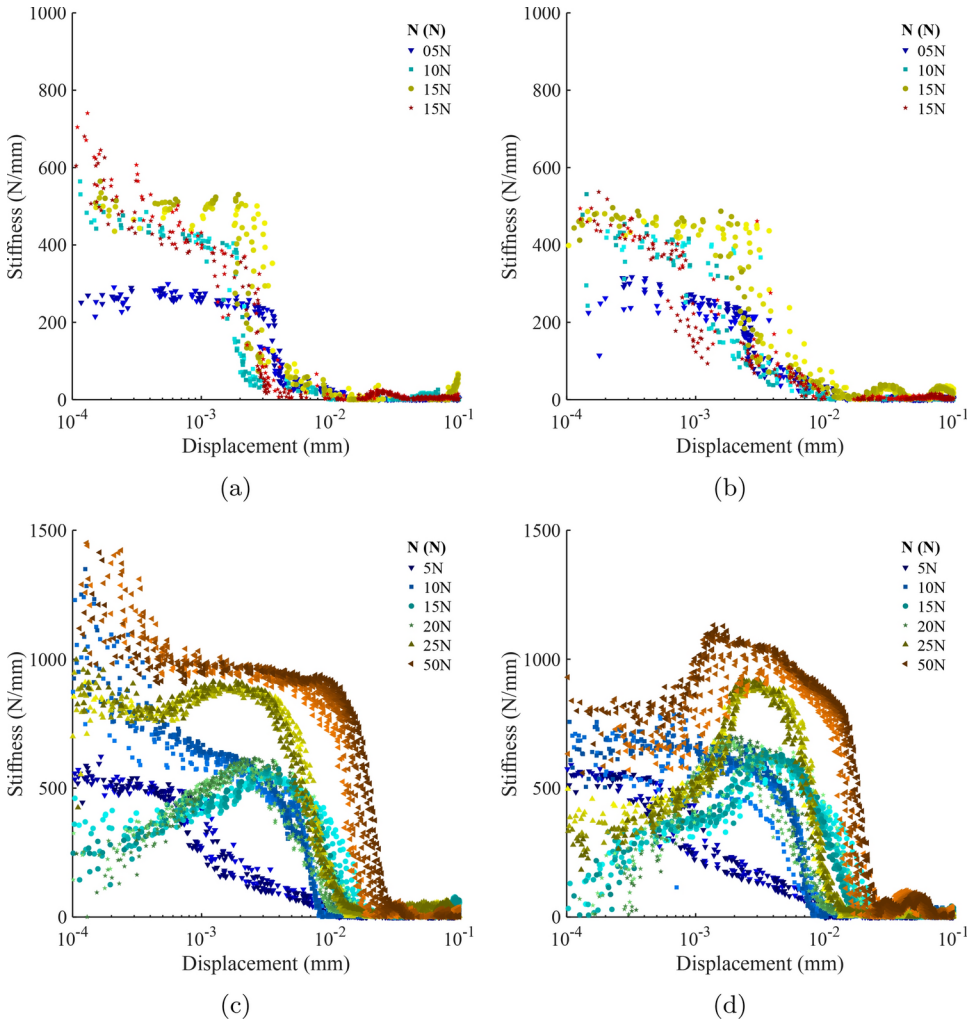

Fig. 11 Cyclic tangential stiffness with displacement. **a** Forward sliding—with shell. **b** Backward sliding—with shell. **c** Forward sliding—core only. **d** Backward sliding—core only. For each load level, cycle number increases from bright to dark colour

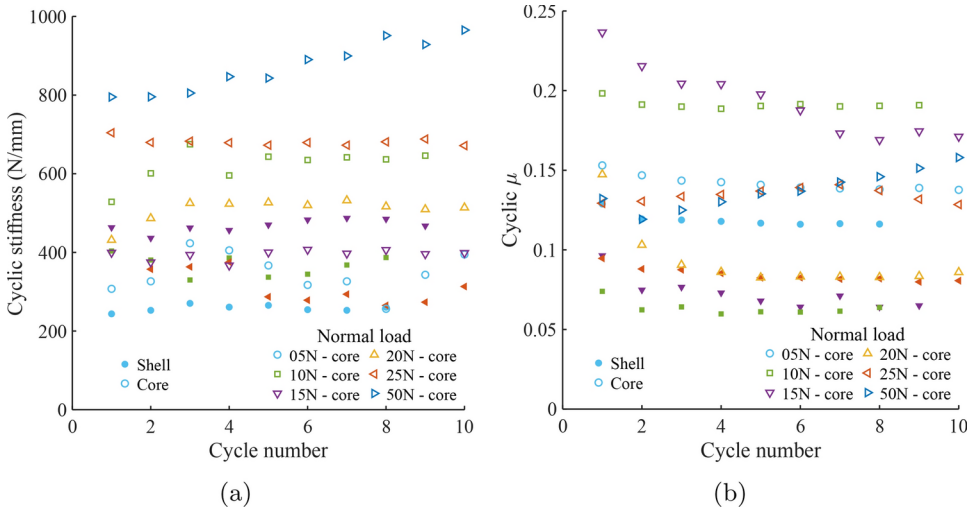

Fig. 12 Cyclic tangential loading tests at different normal loads. **a** Tangential stiffness at 1 μm displacement. **b** μ values

tests than tests done with shells. The effects of load level and whether the shell is present or not are therefore consistent between the monotonic tests (Fig. 9) and the cyclic (Fig. 12).

8 Insights into modelling the particulate behaviour of lentils

The shell of lentils is very compliant before the transition; the deformation of shell until transition is about half of the total deformation of the lentil prior to damage to the core at loads which are $\frac{1}{400}^{\text{th}}$ to $\frac{1}{200}^{\text{th}}$ of the load at damage (Fig. 2). For transition from shell to core dominated response, either shell must rupture and not contribute to resisting the deformation or shell should have much higher stiffness than core post transition point for core to deform. The deformation of the shell is elastic, as shown in Fig. 6b, which implies that the shell does not rupture to a very high load. This suggests that the stiffness of the shell after transition becomes significantly higher than that of the core. Further, to check if stiffness in shell response before transition was dependent on the thickness of the shell, the thickness of the shell of each lentil was measured using a micrometer. Figure 13a shows that shell stiffness is not correlated with the thickness of the shell; for all practical purposes, the stiffness of the shell before transition can be assumed to be constant. Assuming that the stiffness of the shell after transition is infinite (significantly higher than the core), the contact behaviour of lentils in normal loading can be modelled as the following (Fig. 13b):

$$F = \begin{cases} k_{shell}\delta & \text{for } \delta \leq \delta_t \quad (4a) \\ k_{core}\left(\delta - \delta_t + \delta_{ct}\right)^p & \text{for } \delta > \delta_t \quad (4b) \end{cases}$$

where k_{shell} is the stiffness of the shell; k_{core} and p are the power law coefficient and exponent for core response; δ is the deformation of lentil, δ_t is the deformation of lentil at transition, and δ_{ct} is the deformation of the core at transition,

$$\delta_{ct} = \left(\frac{k_s \delta_t}{k_c}\right)^{\frac{1}{p}} \quad (5)$$

Figure 13c shows the distribution of exponent p for all the tests performed in this study. The median value of the exponent was 1.58 which is quite close to the exponent in Hertz model (1.5). Also, as discussed earlier, the Hertz contact model predicts the response of the core quite well (Fig. 4d). Without loss of significant accuracy, equation 5 can be replaced with the Hertz contact equation and k_{core} can be obtained from effective radius of contacting bodies and effective elastic moduli. With this in view, the contact model in normal loading can be written as follows:

$$F = k_{Hertz}\left(\delta - \delta_t + \delta_{ct}\right)^{\frac{3}{2}} \qquad \text{For } \delta > \delta_t \quad (6)$$

where k_{Hertz} is given by $\frac{4}{3}E^* R^{1/2}$ with $\frac{1}{E^*} = \frac{1-\nu_1^2}{E_1} + \frac{1-\nu_2^2}{E_2}$ and $\frac{1}{R} = \frac{1}{R_1} + \frac{1}{R_2}$; ν_i, E_i, R_i are the Poisson's ratio, elastic modulus, and radius (at the contact) of the contacting particles.

The stiffness of the shell (average—3.26 N/mm) reported in Sect. 4 is the equivalent stiffness of either two lentil shell-platen contact or one shell–shell contact. The stiffness of the individual shell should be twice the equivalent stiffness (as $1/k_{eq} = 1/k + 1/k$), i.e., 6.52 N/mm, and transition displacement of the individual shell should be half the equivalent transition displacement (0.128 mm), i.e., 0.064 mm. Further, the average stiffness of lentil core response (after transition) is found to be 1.5 times k_{Hertz} as shown in

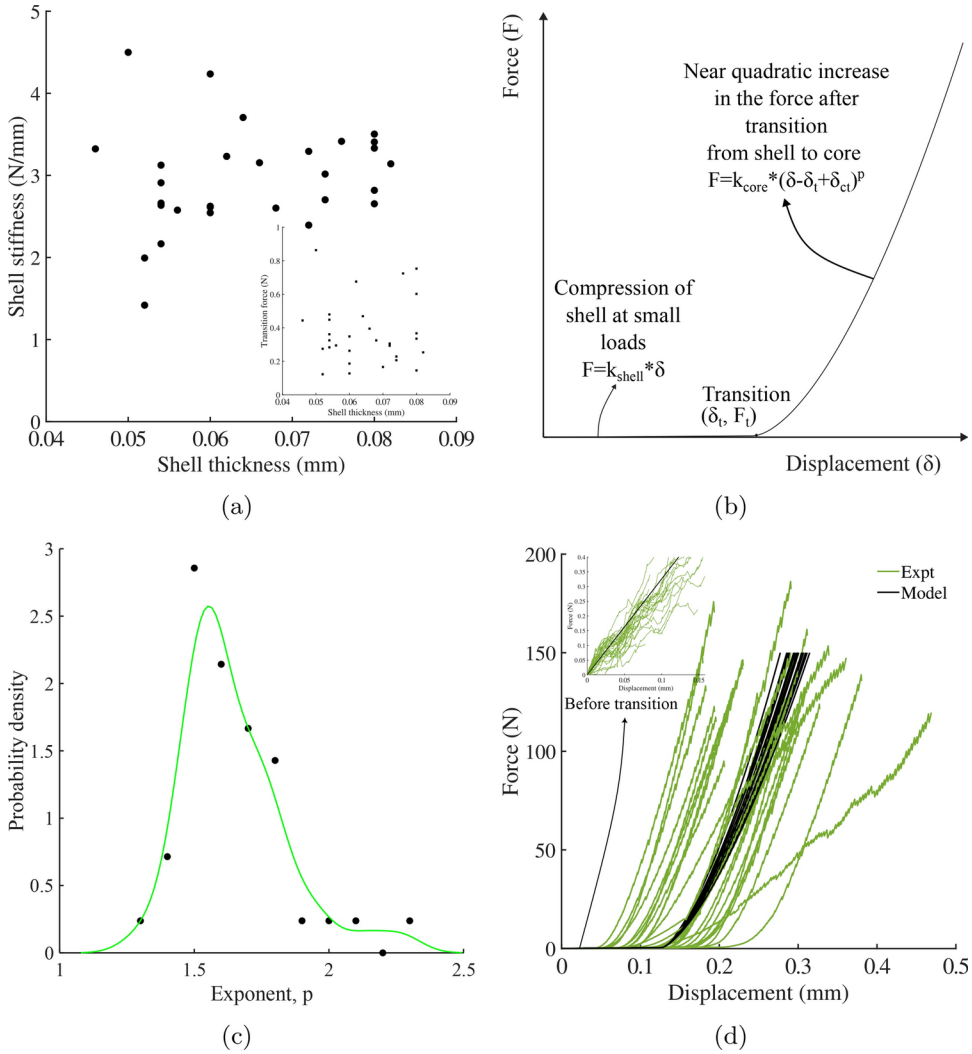

Fig. 13 Normal contact behaviour of lentil particles. **a** Shell stiffness with shell thickness. **b** A simple contact model. **c** Probability density of p (exponent for core). **d** Comparison with predicted response

Fig. 4d. This implies that the elastic modulus for lentil, as suggested in [24], is less than the actual modulus; the elastic modulus for predicting the response of lentil is taken as 1800 MPa (1.5 times 1200 MPa) with Poisson's ratio of 0.30. Using the equation 4a, Eq. 6 and the above parameters, the response of lentil in compression is compared with proposed simple model in Fig. 13d. This simple model predicts the response after transition quite well; however, as there is quite a lot of scatter in transition displacement, only average behaviour is predicted prior to transition with a simple deterministic model.

Figure 14 shows the linear fit for coefficient of static friction with normal load and tangential stiffness with normal stiffness for different normal loads. In the tangential shearing, the coefficient of static friction decreases with normal stiffness (Fig. 14a) and initial tangent stiffness increases with normal stiffness (or load) (Fig. 14b) with following relations (for 0 N to 25 N normal load):

$$\mu_s = -0.0042N + 0.34 \tag{7}$$

$$k_T = 0.52k_{Hertz} \tag{8}$$

Where k_{Hertz} is the stiffness calculated using Hertz model for a constant normal load (N) with the expression $\left(6NRE^{*2}\right)^{1/3}$.

Further, The reduction in tangential stiffness with tangential displacement (t) can be modelled using Mindlin and Deresiewicz equation [30] as

$$\frac{dT}{dt} = k_T\left(1 - \frac{T}{\mu_s N}\right)^{1/3} \tag{9}$$

For tangential sliding at constant normal load, the tangential force can be integrated from Eq. 9

$$T = \mu_s N\left[1 - \left(1 - \frac{2k_T t}{3\mu_s N}\right)^{3/2}\right] \tag{10}$$

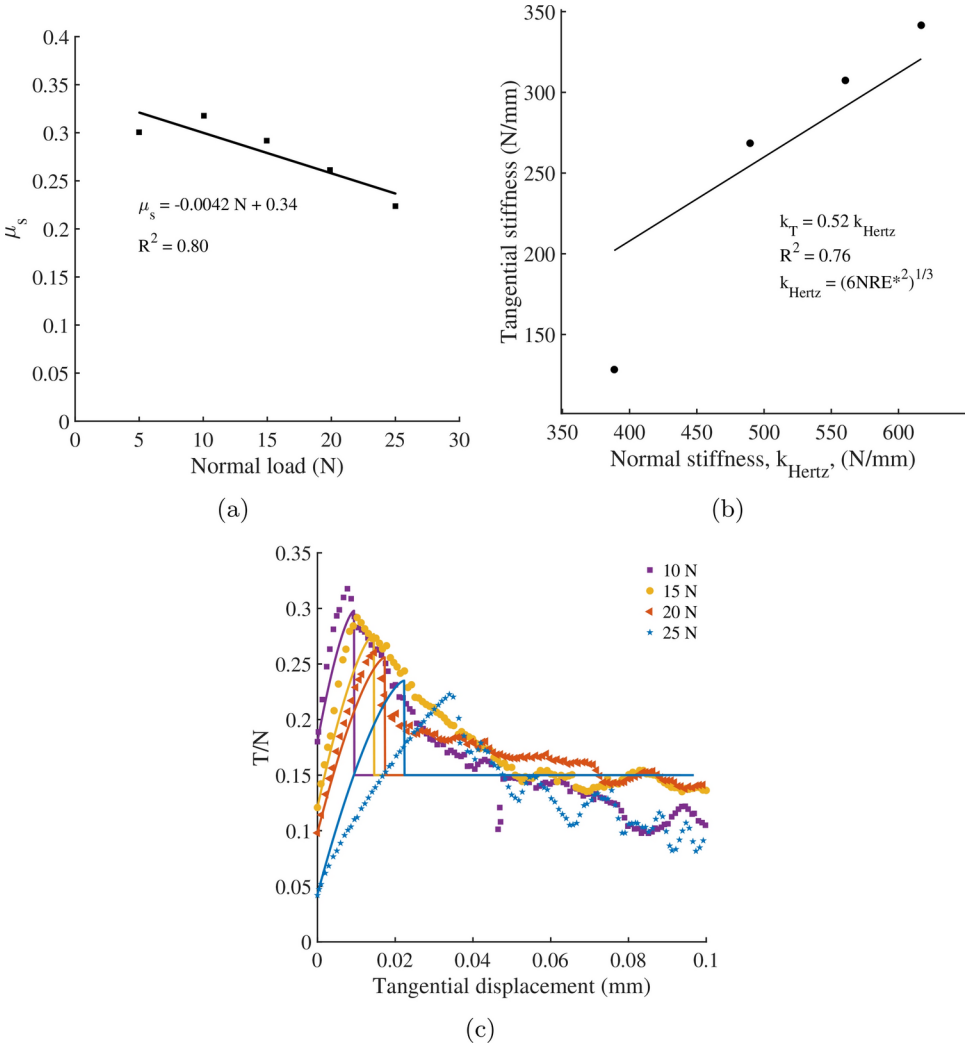

Fig. 14 Tangential contact behaviour of lentil particles with shell. **a** Coefficient of friction with normal load. **b** Tangential stiffness with normal stiffness calculated using Hertz model. **c** Prediction of tangential force response

Using the above relation along with Eqs. 7 and 8, the response of tangential sliding is predicted and compared in Fig. 14c. As discussed earlier, tangential response starts at non-zero tangential load due to partial mobilization of tangential force in the vertical loading; predicted response (particularly, tangential displacement) is adjusted to start at identical non-zero tangential load.

This simple model, for normal and tangential contact behaviour of lentil, can be used to simulate the response of lentils under different boundary conditions in discrete element modelling. The contact model from this study along with fabric and its evolution from Pinzon et al. [11] also provides a complete dataset for characterisation of DEM algorithms.

9 Conclusions

Lentils show a multifaceted behaviour due to the presence of skin or shell, which acts as a protective layer for the core. At small deformation, lentil response is linear and governed by the compression of skin, which has stiffness of 3 N/mm. With increase in deformation, a transition is observed at 0.1 mm to 0.2 mm displacement, after which the lentil response is quite stiff; a power law increase in the force is observed with the displacement. The post transition response is akin to core-core contact response without the presence of shell. Even at very high loads, the shell of lentil deforms elastically, with a relatively high stiffness after the transition, which leads to significant deformation of the core. The lentil behaviour in normal load can be modelled by a linear response before the transition and by the Hertz model after the transition.

Under load reversal and cyclic loading, lentils show plastic yielding and fatigue. Lentils accumulate plastic deformation at each cycle, until plastic shakedown. The secant stiffness increases with cycle number and approaches a steady state at around 60 to 80 cycles. The damping shows a similar response with steady state at 20 to 30 cycles. The cyclic secant stiffness increases and damping decreases with mean normal load.

In tangential sliding, the coefficient of friction between a pair of lentil particles decreases linearly with increase in normal load, whereas tangential stiffness increases linearly with normal stiffness. The repeated forward and backward sliding also affects the coefficient of friction. The presence of skin or shell reduces both coefficient of friction and cyclic tangential stiffness.

A simple model was proposed, but overall, the insights obtained in this study of lentils should be very useful for discrete element modelling better adopted to lentils under different loading conditions.

Acknowledgements The authors are grateful for the technical support of Mr. Matt Wilkinson in supporting our research, and to Professor G. Viggiani of the Université Grenoble Alpes who supplied the lentils. The work was wholly funded by EPSRC Project No. EP/W000563/1.

Author contributions S.S. and B.A.B. wrote the original draft of the manuscript. S.S., B.A.B. and M.R.C planned the experiments. S.S. carried out the experiments. S.S., B.A.B., and M.R.C. analysed and discussed the data. S.S. performed the analysis and plotted the figures. S.S., B.A.B., and M.R.C. edited and revised the manuscript for final submission. B.A.B and M.R.C acquired the funding to carry out the research.

Funding This research work was wholly funded by EPSRC Project No. EP/W000563/1.

Data availability Data is provided within the manuscript in the form of plots.

Declarations

Conflict of interest The authors declare that they do not have any Conflict of interest as defined by Springer, or other interests that might be perceived to influence the results and/or discussion reported in this paper.

Ethical approval Not Applicable

References

1. FAO: Agricultural Production Statistics 2000-2021. Faostat Analytical Brief Series, vol. 60. FAO, Rome, Italy (2022). https://doi.org/10.4060/cc3751en
2. Rivera, J.L., Zhao, J., Owonikoko, A., Siliveru, K.: Significance of storage conditions on the flow properties of wheat flours. J. Food Meas. Char. **17**(5), 4394–4404 (2023). https://doi.org/10.1007/s11694-023-01938-0
3. Hall, D.W.: Handling and Storage of Food Grains in Tropical and Subtropical Areas. FAO Plant Production and Protection Series No. 19, vol. FAO Agricultural Development Paper No. 90. Food & Agriculture Organisation, Rome, Italy (1970)
4. FAO: In: Mrema, G.C., Gumbe, L.O., Chepete, H.J., Agullo, J.O. (eds.) Rural structures in the tropics: design and development, pp. 363–385. Food and Agriculture Organization of the United Nations, Rome, Italy (2011). Chap. 16
5. Santamarina, J.C., Cho, G.C.: Soil behaviour: The role of particle shape, pp. 604–617. https://doi.org/10.1680/aigev1.32644.0035 . https://www.icevirtuallibrary.com/doi/abs/10.1680/aigev1.32644.0035
6. Altuhafi, F.N., Coop, M.R., Georgiannou, V.N.: Effect of particle shape on the mechanical behavior of natural sands. J. Geotechn. Geoenviron. Eng. (2016). https://doi.org/10.1061/(asce)gt.1943-5606.0001569
7. Cundall, P.A., Strack, O.D.L.: A discrete numerical model for granular assemblies. Géotechnique **29**(1), 47–65 (1979). https://doi.org/10.1680/geot.1979.29.1.47
8. Tolomeo, M., McDowell, G.R.: Modelling real particle shape in dem: a comparison of two methods with application to railway ballast. Int. J. Rock Mech. Min. Sci. **159**, 105221 (2022). https://doi.org/10.1016/j.ijrmms.2022.105221
9. Horabik, J., Molenda, M.: Parameters and contact models for dem simulations of agricultural granular materials: a review. Biosys. Eng. **147**, 206–225 (2016). https://doi.org/10.1016/j.biosystemseng.2016.02.017
10. Hertz, H.: Ueber die berührung fester elastischer körper. Journal für die reine und angewandte Mathematik **1882**(92), 156–171 (1882). https://doi.org/10.1515/crll.1882.92.156
11. Pinzón, G., Andò, E., Desrues, J., Viggiani, G.: Fabric evolution and strain localisation in inherently anisotropic specimens of anisometric particles (lentils) under triaxial compression. Gran. Matter. (2023). https://doi.org/10.1007/s10035-022-01305-8
12. Pan, J.H., Pinzón, G., Wang, R., Andò, E., Viggiani, G., Zhang, J.M.: Lessons learned from matching 3d dem and experiments at macro, meso and fabric scales for triaxial compression tests on lentils. J. Mech. Phys. Solids **183**, 105494 (2024). https://doi.org/10.1016/j.jmps.2023.105494
13. Bargale, P.C., Irudayaraj, J.M., Marquis, B.: Some mechanical properties and stress relaxation characteristics of lentils. Can. Agric. Eng. **36**(4), 247–254 (1994)
14. Shelef, L., Mohsenin, N.N.: Evaluation of the modulus of elasticity of wheat grain. Cereal Chem. **44**(4), 392–402 (1967)
15. Cavarretta, I., O'sullivan, C.: The mechanics of rigid irregular particles subject to uniaxial compression. Géotechnique **62**(8), 681–692 (2012). https://doi.org/10.1680/geot.10.p.102
16. Cavarretta, I., Rocchi, I., Coop, M.R.: A new interparticle friction apparatus for granular materials. Can. Geotech. J. **48**(12), 1829–1840 (2011). https://doi.org/10.1139/t11-077
17. Cavarretta, I., Coop, M., O'sullivan, C.: The influence of particle characteristics on the behaviour of coarse grained soils. Géotechnique **60**(6), 413–423 (2010). https://doi.org/10.1680/geot.2010.60.6.413
18. Senetakis, K., Coop, M.R., Todisco, M.C.: The inter-particle coefficient of friction at the contacts of leighton buzzard sand quartz minerals. Soils Found. **53**(5), 746–755 (2013). https://doi.org/10.1016/j.sandf.2013.08.012
19. Nardelli, V., Coop, M.R.: The experimental contact behaviour of natural sands: normal and tangential loading. Géotechnique **69**(8), 672–686 (2019). https://doi.org/10.1680/jgeot.17.p.167

20. Antonyuk, S., Tomas, J., Heinrich, S., Mörl, L.: Breakage behaviour of spherical granulates by compression. Chem. Eng. Sci. **60**(14), 4031–4044 (2005). https://doi.org/10.1016/j.ces.2005.02.038
21. McDowell, G.R., Bolton, M.D.: On the micromechanics of crushable aggregates. Géotechnique **48**(5), 667–679 (1998). https://doi.org/10.1680/geot.1998.48.5.667
22. McGuiggan, P.M., Wallace, J.S., Smith, D.T., Sridhar, I., Zheng, Z.W., Johnson, K.L.: Contact mechanics of layered elastic materials: experiment and theory. J. Phys. D Appl. Phys. **40**(19), 5984 (2007). https://doi.org/10.1088/0022-3727/40/19/031
23. Bhushan, B., Peng, W.: Contact mechanics of multilayered rough surfaces. Appl. Mech. Rev. **55**(5), 435–480 (2002). https://doi.org/10.1115/1.1488931
24. Rataj, V.: Poisson's constant determination of selected legumes and oil seeds. Int. Agrophys. **8**(2), 295–298 (1994)
25. Wong, C., Boorman, B., Coop, M.: The construction and commissioning of a new inter-particle loading apparatus for the micro-mechanical behaviour of railway ballast. In: Proceedings of IS Atlanta 2018 Symposium on Geomechanics from Micro to Macro in Research and Practice (2019)
26. Wong, C.P.Y.: Micro-mechanical contact behaviour for railway ballast. PhD thesis, University College London (2022). https://discovery.ucl.ac.uk/id/eprint/10145756
27. Wang, W., Coop, M.R.: An investigation of breakage behaviour of single sand particles using a high-speed microscope camera. Géotechnique **66**(12), 984–998 (2016). https://doi.org/10.1680/jgeot.15.p.247
28. Nakata, A.F.L., Hyde, M., Hyodo, H.: Murata: a probabilistic approach to sand particle crushing in the triaxial test. Géotechnique **49**(5), 567–583 (1999). https://doi.org/10.1680/geot.1999.49.5.567
29. Nakata, Y., Hyodo, M., Hyde, A.F.L., Kato, Y., Murata, H.: Microscopic particle crushing of sand subjected to high pressure one-dimensional compression. Soils Found. **41**(1), 69–82 (2001). https://doi.org/10.3208/sandf.41.69
30. Mindlin, R.D., Deresiewicz, H.: Elastic spheres in contact under varying oblique forces. J. Appl. Mech. **20**(3), 327–344 (1953). https://doi.org/10.1115/1.4010702